Supporting Information for:

Understanding Why Poly(Acrylic Acid) Works: Decarbonylation and Cross-Linking Provide an Ionically Conductive Passivation Layer in Silicon Anodes

Trevor R. Martin, Ryan T. Pekarek, Jaclyn E. Coyle, Maxwell C. Schulze, Nathan R. Neale*

Chemistry and Nanoscience Center, National Renewable Energy Laboratory, Golden, CO, 80401, USA. E-mail: nathan.neale@nrel.gov

CBT Film preparation

Binder solutions were prepared by dissolving 100 mg of 450 k Mw Poly(acrylic acid) binder in 5.0 mL anhydrous *N*-Methyl-2-pyrrolidone (NMP). For the 10% esterified binder, 15 µL pentanol was added to the solution and the mixture was heated to 100 °C with stirring and was concurrently sparged with dry nitrogen for 60 min to remove water. For the 20% esterified binder, 30 µL pentanol was added to the solution and the mixture was heated to 100 °C with stirring and was concurrently sparged with dry nitrogen for 60 min to remove water. The binder films were deposited onto (100) silicon wafers purchased from Addison Engineering (0.002Ω cm, boron-doped, 675 µm thick, single-side polished) cut into approximately 5 cm x 5 cm sized pieces by drop casting 1.0 mL of the solutions. The films were then placed in a vacuum oven and cured for 12 h at 150 °C.

The films were removed from the vacuum oven and were adhered to an aluminum block using 3M™ Scotch-Weld™ DP420 epoxy adhesive. A titanium beam (dimensions: 0.8 mm x 5.0 mm x 100 mm) was adhered to the PAA or E-PAA surface using 3M™ Scotch-Weld™ Structural Plastic DP8005 epoxy adhesive. Specifically, a thin epoxy coating was deposited onto the surface of the titanium beam and the beam was gently pressed onto the binder coating. After curing for 12 h, the titanium beams were connected to a load cell affixed to a linear actuator.

CBT measurement Techniques

First, the average spring constant of the titanium beams was measured at a range of fixed debond lengths (a) as shown in (Figure S1a). Four different titanium beams (including those with and without an epoxy coating) were tested to determine the inherent errors in this calculation. The linear relationship between the square of the debond length (a^2) and the beam compliance was subsequently determined (Figure S1a) using a fitting algorithm written in Python 3.7.7.

Next, a CBT sample was tested by pulling upward on the titianium beam at a constant rate while measuring the applied load as shown in Figure S1 until the binder layer was eventually debonded from the silicon interface (a debond event), generating a yield point as seen in Figure S1b. An algorithm was written in Python 3.7.7 and was used to determine yield points and to extract the linear fits of the data as shown in Figures S1c and S1b before failure, thereby generating a compliance value. This compliance value was then used to determine an effective debond length using the linear relationship from Figure S1a. This effective debond length was then combined with the yield point force to calculate an effective debond energy.[1,2] Each sample generates data from several debond events and multiple samples were tested to generate the mean and standard deviation values for the debond energy as a function of esterification as presented in Figure S3.

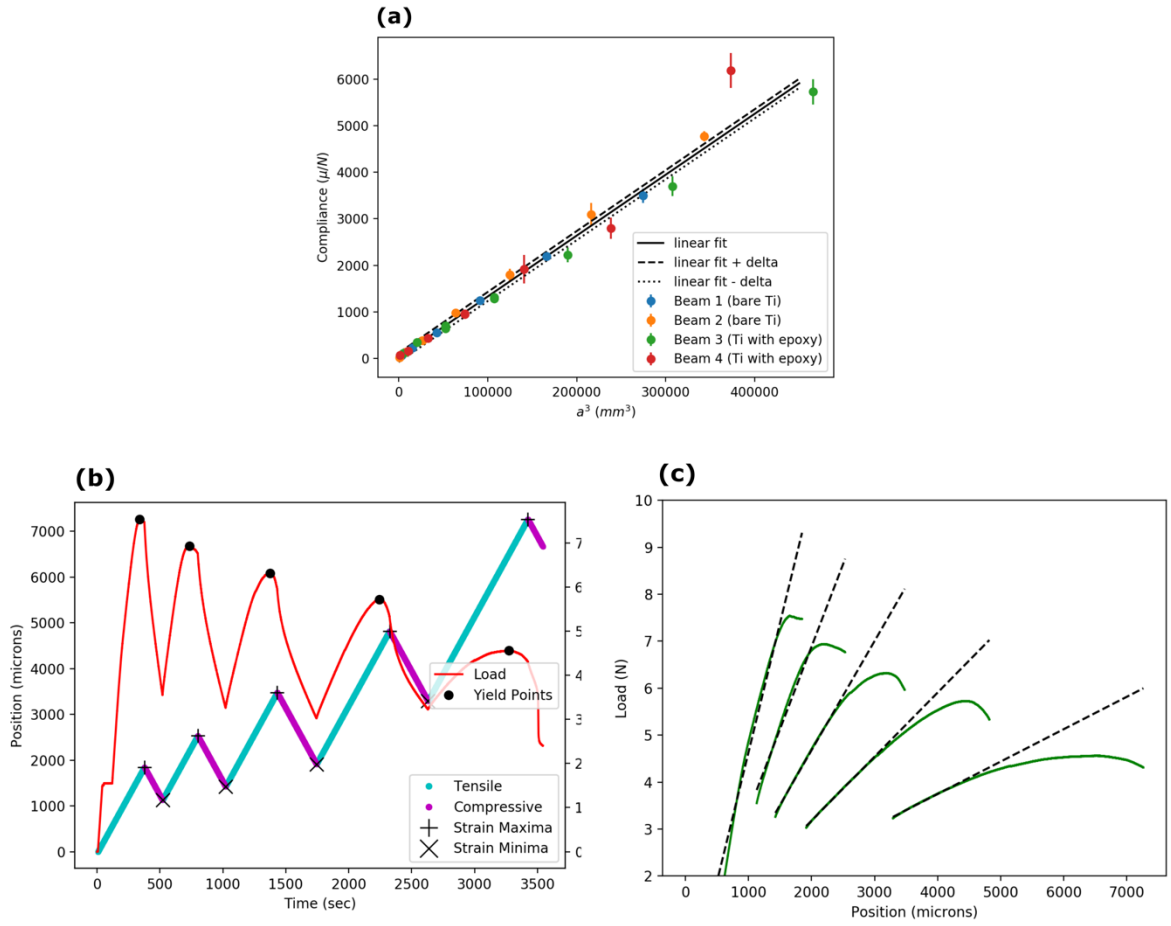

Figure S1. a) Normalization data from four different titanium beams, where the linear relationship between the square of a fixed dedond length and a measured compliance value was determined. b) Example dataset that has been analyzed using the algorithm to determine yield points and debond event regions. c) Example dataset that has been analyzed by the algorithm to determine the compliance value of the titanium beam before a debond event.

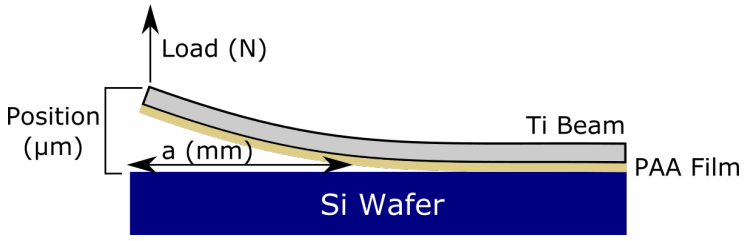

Figure S2. Experimental setup for the cantilever beam test (CBT), where the adhesive properties of a PAA or E-PAA film are determined by mechanically peeling the polymer film away from the silicon surface. The displacement, load, and mechanical properties of the titanium beam are subsequently measured to calculate the debond energy.

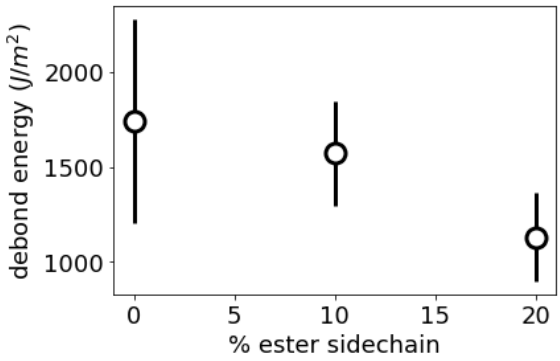

Figure S3. Cantilever beam test (CBT) data showing that as the carboxyl moieties in the PAA binder are deactivated via esterification, then there is a systematic decrease in adhesion strength to a silicon wafer.

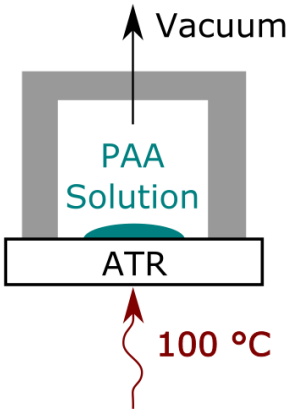

Figure S4. Design of in situ infrared spectroscopy binder drying experiment used to collect data in Figure 1. Samples were prepared by adding 38 µL or 76 µL pentanol (E-PAA (25%) or E-PAA (50%) respectively) to 100 mg of 450k MW PAA dissolved in 5 mL deionized water. The solutions were stirred at 300 rpm and heated to 50 ºC for 60 minutes before depositing 1 mL onto the ATR crystal via drop casting.

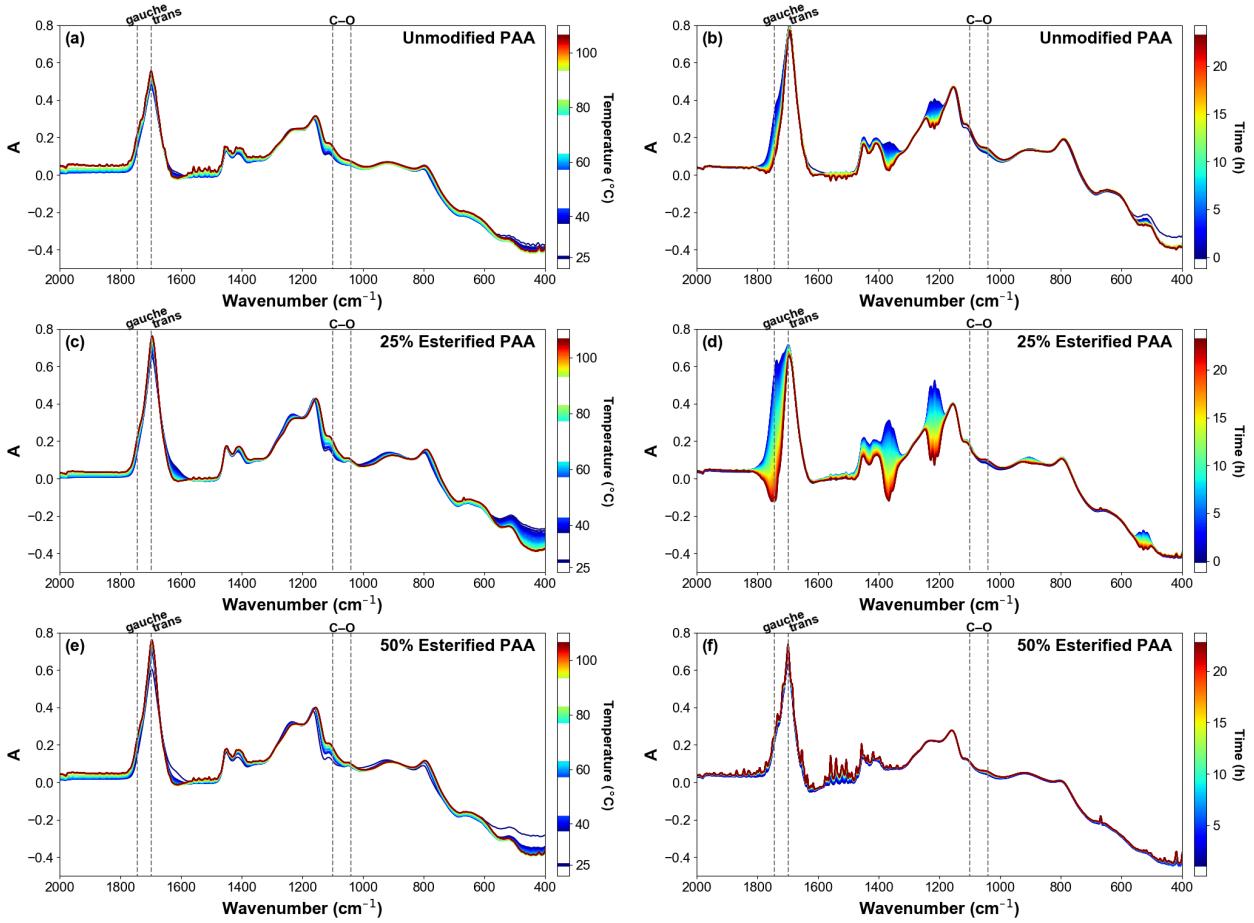

Figure S5. Full infrared spectroscopy of binder drying data presented in Figure 1. Variable temperature spectra during temperature increase from room temperature to 100 °C (a,c,e). Spectra collected at 100 °C during 24 h drying experiment (b,d,f). Three polymers are shown: unmodified PAA (a,b); 25% esterified PAA (c,d); 50% esterified PAA (e,f).

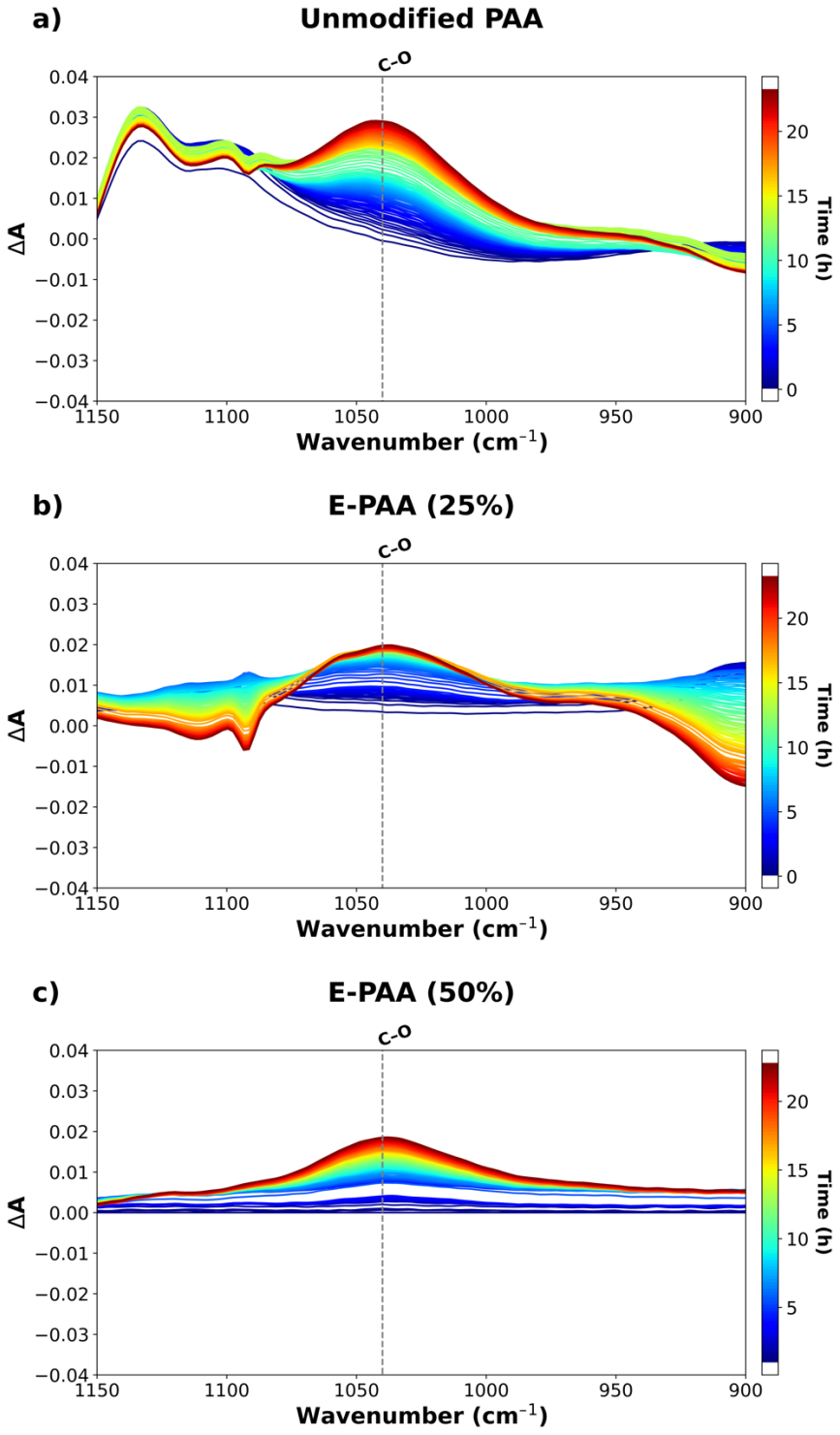

Figure S6. In situ infrared spectroscopy of the binder drying data collected at 100 °C during the 24 h drying experiment. These spectra are analogous to those presented in Figure 1 but are focused on the C-O bond region. Three polymers are shown: unmodified PAA (a); 25% esterified PAA (b); 50% esterified PAA (c). All spectra are difference spectra, and unsubtracted spectra are shown in Figure S5.

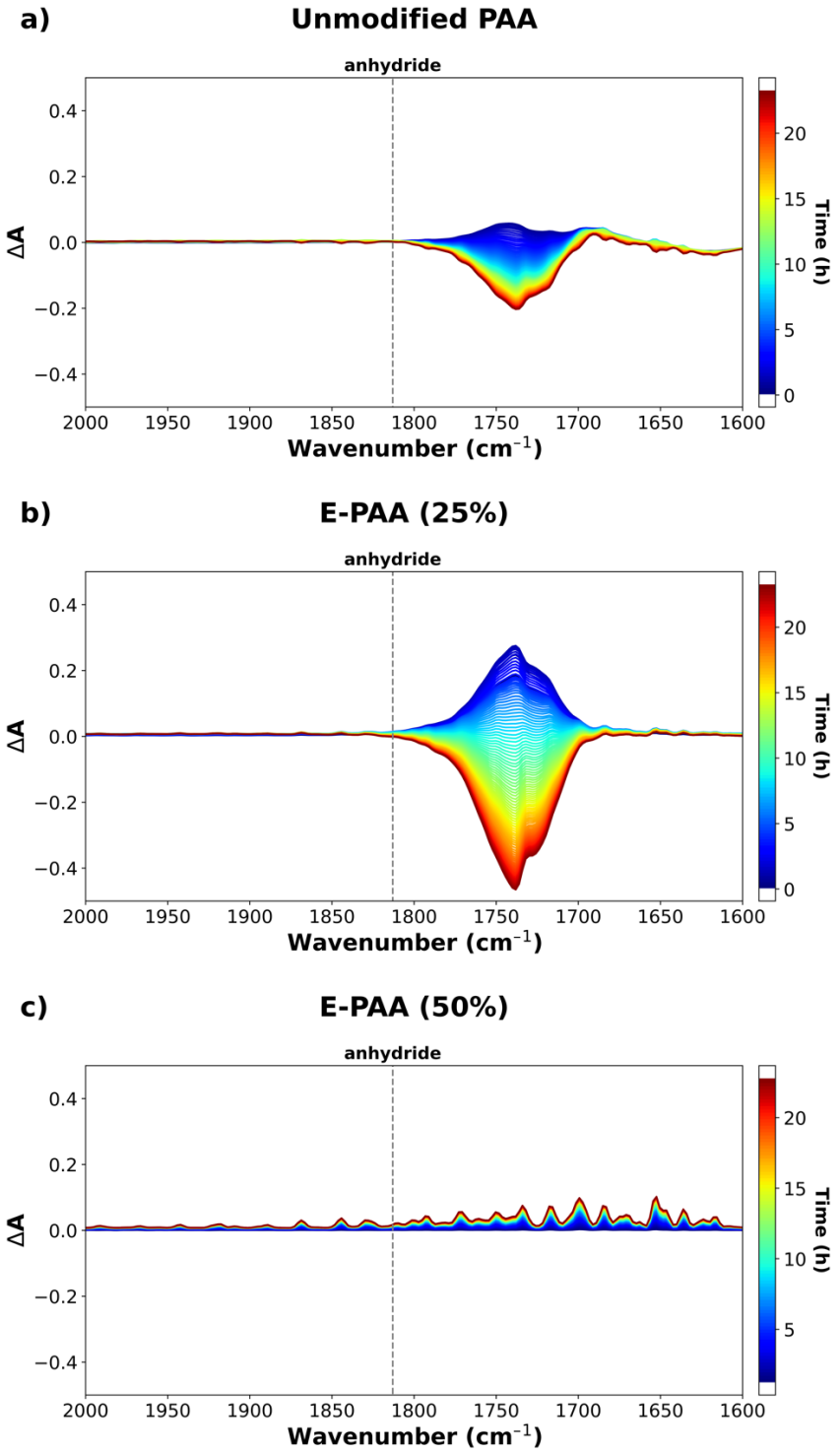

Figure S7. In situ infrared spectroscopy of the binder drying data collected at 100 °C during the 24 h drying experiment. These spectra are analogous to those presented in Figure 1 but are focused on the 1600–2000 cm^{-1} bond region to highlight the absence of anhydride moieties, which would be expected between 1800–1820 cm^{-1} denoted by the dashed gray vertical line. Three polymers are shown: unmodified PAA (a); 25% esterified PAA (b); 50% esterified PAA (c). All spectra are difference spectra, and unsubtracted spectra are shown in Figure S5.

Ex Situ PAA Film Fabrication and Analysis

In addition to the in situ methods presented herein, we also fabricated a standalone PAA film for ex situ ATR-FTIR spectroscopic analysis. To fabricate these films, we first drop-cast 250 µL of PAA solution (100 mg of 450k MW PAA dissolved in 5 mL deionized water) onto a Ge ATR crystal and then dried the film at 100 °C for 24 h in a vacuum oven (roughing pump pressure ~10^{-2} Torr). The film was subsequently analyzed using ATR_FTIR spectroscopy (Figure S8). Next, the film and Ge ATR stage were reinserted into the vacuum oven and processed at 150 °C for 3 h. Finally, the film was reanalyzed to observe changes in the spectra at the higher processing temperature (Figure S8). The spectra show residual signals from water since they were analyzed in open air. We note that the 150 °C spectrum shows a small peak near the anhydride region (~1800 cm^{-1}) that is slightly enhanced beyond the background signal and is not easily comparable to the 100 °C data without the accuracy afforded by the in situ difference spectra technique. This is a possible indication of a small proportion of (intermediary or otherwise) anhydride formation during this relatively short reaction time (3 h). Therefore, when compared to the strength and clarity of the ether signal and when combined with our in situ data, we hypothesize that the anhydride is likely not the dominant moiety that is formed in the composite Si electrodes. Most importantly, the 150 °C data show an increase in polyether formation peak at ~1050 cm^{-1} when compared to the 100 °C spectrum.

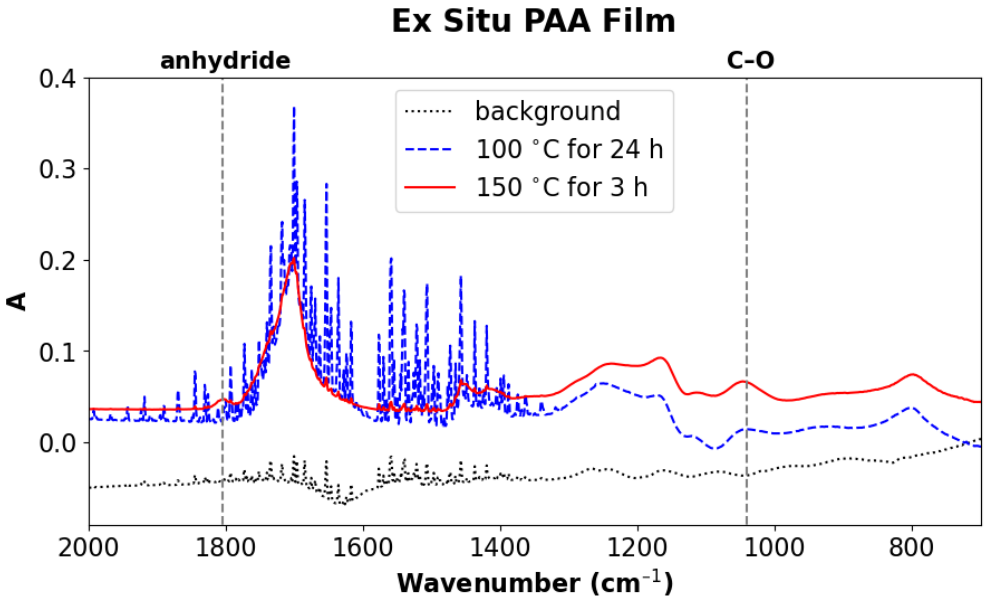

Figure S8. Ex situ infrared spectroscopy of a PAA film collected after vacuum drying at 100 °C for 24 h (blue trace) and then 150 °C for 3 h (red trace).

Polymer Tacticity Discussion

The degree of polymer esterification also impacts the relative ratio of the gauche and trans isomer conformations present in Figures 1a, 1c, and 1e. Specifically, these spectra show that as the degree of esterification increases there is a concurrent and proportional growth in the trans isomer peak. These results indicate that as the carboxyl moieties react to form an ester side chain, then the polymer side chain orientation changes due to steric hindrance and the ester side chains

become less reactive to future condensation and decarbonylation reactions. In addition, these data support our assumptions for the relative proportions of esterified side-chains in the polymers (m to n ration in Scheme 1). Accordingly, the esterification process also directly impacts polymer tacticity. The E-PAA (50%) spectra shown in Figure 1f show a series of small peaks that can be attributed to residual water that is trapped in the film. We postulate that since this film undergoes the least amount of cross-linking, then it will have proportionally more ester groups in comparison to the E-PAA (25%) and PAA films, which will cause the film to be slightly more polar and subsequently more hydrophilic. Furthermore, the C-O peaks in the 1050 cm^{-1} region for E-PAA (50%) (Figure 1f) are the least pronounced of the three polymer films, which also supports our hypothesis.

Nanoindentation of Composite Anodes

Nanoindentation tests were conducted using a KLA iMicro Nanoindenter equipped with a diamond Berkovich indenter tip inside an inert atmosphere glovebox. Thermal drift during indentation was maintained below 0.5 nm/s. Depth controlled tests with a constant strain rate of $0.05s^{-1}$ were used with a 10s hold at maximum load. The maximum depth was chosen such that it did not exceed greater than 1/10 the total thickness of the electrode to eliminate any effects from the copper substrate. The Oliver-Pharr method was followed to determine the elastic modulus and hardness of the material.[3]

Fig S9. The average elastic modulus determined by nanoindentation for composites with varying esterification based on 20 indents.

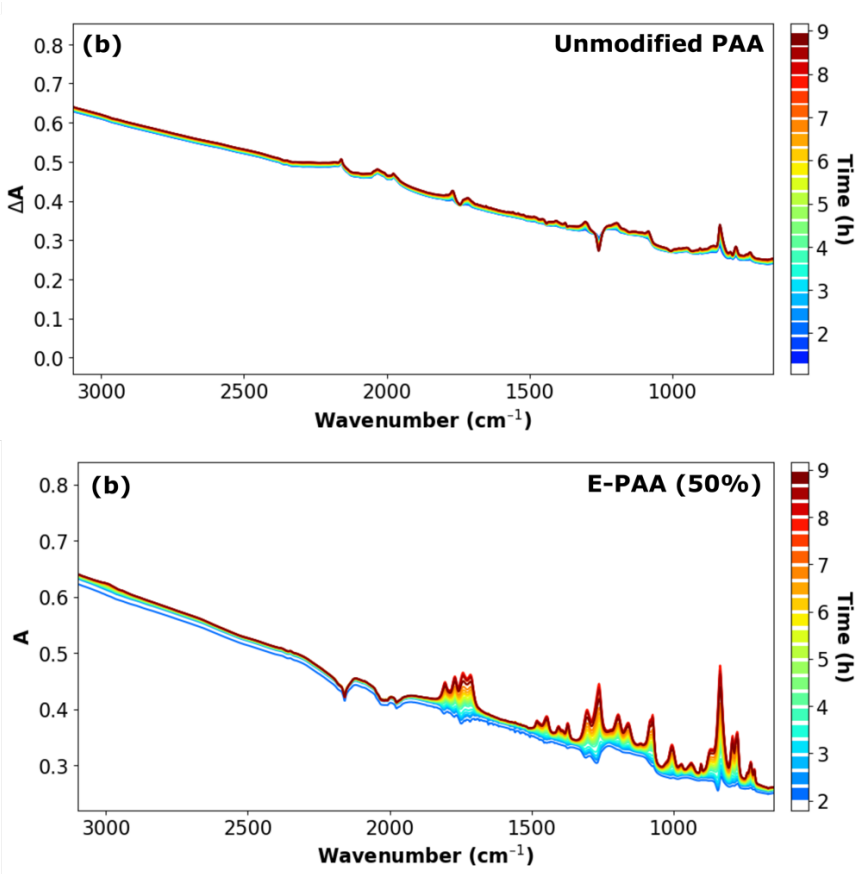

Figure S10. Full in situ spectra during open circuit voltage hold (OCV) for unmodified PAA (a) and E-PAA (50%) (b) binders for the data presented in Figure 4.

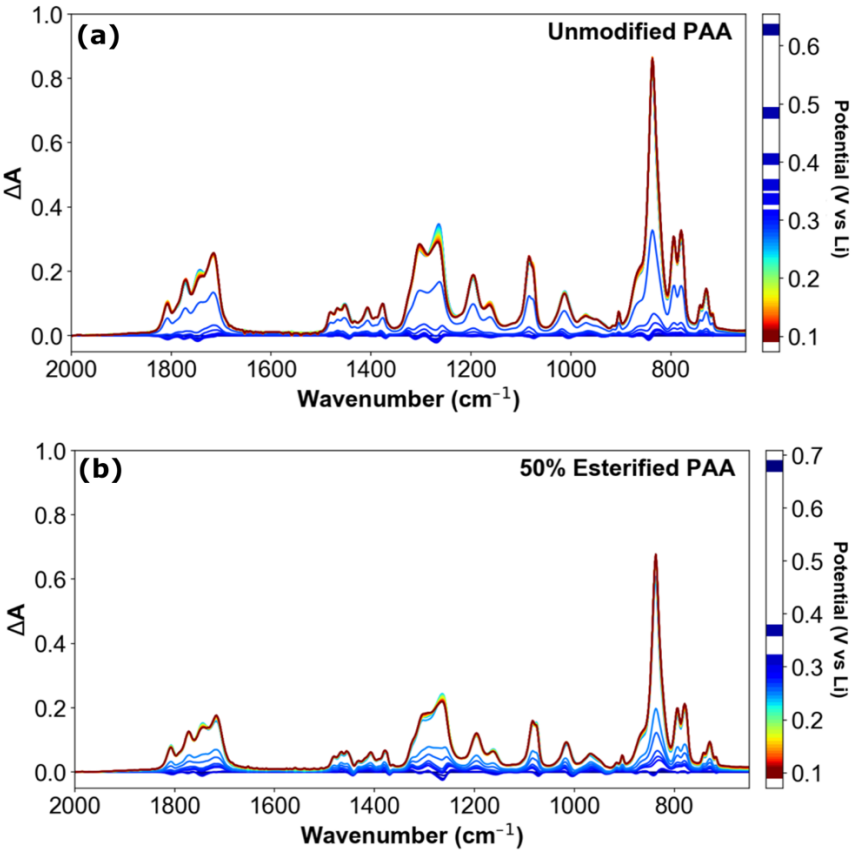

Figure S11. Full in situ spectra for the data presented in Figure 6 for electrodes during the first lithiation using either E-PAA (50%) (a) or unmodified PAA (b) binders.

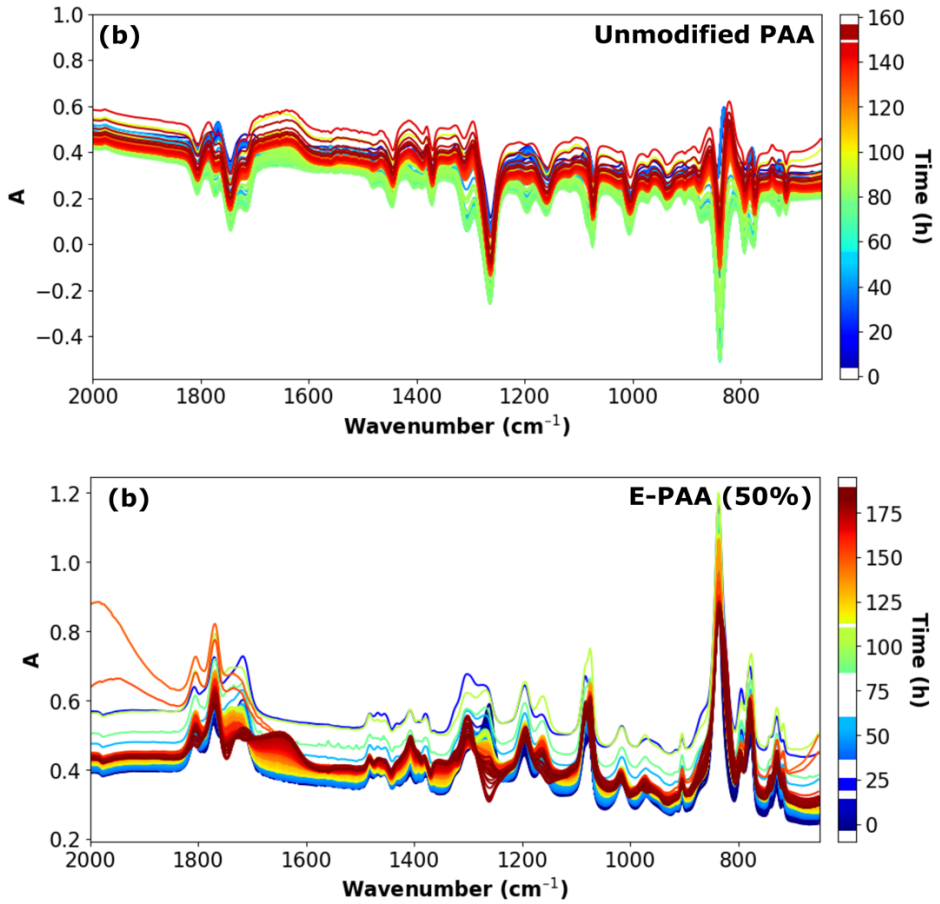

Figure S12. Full spectra for the data presented in Figure 6 during a 100 mV potential hold using either E-PAA (50%) (a) or unmodified PAA (b) binders.

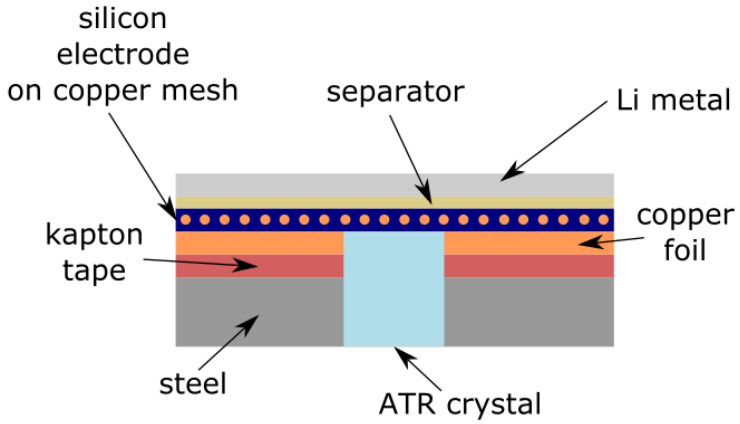

Figure S13. Design of infrared spectroelectrochemical experiment used to collect data shown in Figures 4-6.

References

(1) Bosco, N.; Moffitt, S.; Schelhas, L. T. Mechanisms of Adhesion Degradation at the Photovoltiac Module's Cell Metallization-Encapsulant Interface. *Prog. Photovoltaics Res. Appl.* **2019**, *27* (4), 340–345. https://doi.org/10.1002/pip.3106.

(2) Bosco, N.; Tracy, J.; Dauskardt, R. Environmental Influence on Module Delamination Rate. *IEEE J. Photovoltaics* **2019**, *9* (2), 469–475. https://doi.org/10.1109/JPHOTOV.2018.2877436.

(3) Oliver, W. C.; Pharr, G. M. Measurement of Hardness and Elastic Modulus by Instrumented Indentation: Advances in Understanding and Refinements to Methodology. *J. Mater. Res.* **2004**, *19* (1), 3–20. https://doi.org/10.1557/jmr.2004.19.1.3.